

Micromachined high gain wideband antennas for wireless communications

Sumanth K. Pavuluri, Changhai Wang and Alan J. Sangster
*Heriot Watt University
Edinburgh, EH14 4AS, UK*

1. Introduction

The seemingly insatiable and growing demand for compact, multi-function, multi-frequency electronic systems for communications and other applications, is continuing to drive the search for devices offering more and more bandwidth. There is growing need for broadband high gain communication systems in the X band range of frequencies (8 - 12 GHz) for terrestrial broadband communications and networking as well as for radar applications. Similarly, direct broadcast satellite (DBS) and various other applications in the K_u band (10 - 14 GHz) such as radio astronomy service, space research service, mobile service, mobile satellite service, radio location service (radar), amateur radio service, and radio navigation may require embedded antenna systems at different bands. It would be ideal if efficient, broadband and cost effective planar microstrip based antenna and antenna array devices could be designed to provide coverage of all these bands. In addition systems aimed at UWB (Ultra Wide Band) operation need efficient very wideband antenna devices.

For these high frequency systems, compact size and high performance can usually be achieved by fabricating the antenna onto a low dielectric constant material and integrating it with the remaining circuitry implemented on a high dielectric constant substrate in neighbouring regions in the same package. This trend has serious implications for antennas, where these are required to be embedded within the system package, such as a mobile phone. Systems operating in the microwave and millimetre-wave frequency bands offer the possibility of high levels of integration of individual devices in high density layouts. The most compact circuit designs are invariably achieved by employing high dielectric constant substrates, but this is a requirement which is essentially incompatible with the needs of an embedded planar antenna. Such antennas radiate most efficiently when fabricated onto substrates which exhibit low dielectric constant (Papapolymerou et al., 1998). While it is not impossible to fabricate microstrip or coplanar circuits, together with planar antennas on the same high permittivity silicon substrate, antenna gain and efficiency will inevitably be very poor.

Various schemes have been suggested, in recent years, aimed at overcoming the opposing substrate requirements of circuits and antennas. These largely involve the use of layered materials with high and low permittivities in adjacent layers (Chen, 2008). However such

methods tend to be of quite limited versatility and the trend now is toward selective removal of substrate in the vicinity of the antenna. This can be done by, for example, bulk micromachining an air gap between the planar antenna (usually a conducting patch) and the ground plane (Koul, 2007). The advantages of doing so are as follows:

- Lower effective dielectric constant, hence wider circuit dimensions
- Ease of fabrication and relaxed dimensional tolerances
- Lower attenuation
- Enhanced radiation efficiency in case of antennas
- Eliminating surface waves

Micromachining technology continues to develop, and it is being applied in new ways to embedded antennas to improve their performance. The use of selective lateral etching based on micromachining techniques to enhance the performance of rectangular microstrip patch antennas printed on high-index wafers such as silicon, GaAs, and InP have been developed in the past decade. A novel polymer micromachining based method for achieving high performance, cost effective antennas is described in this chapter.

2. Micromachined antennas

Over the last decade several micromachining techniques have been developed for producing microwave wave and millimeter wave antennas. Devices using these procedures have achieved high performances compared to the conventional patches printed on to relatively high dielectric constant substrates. Various micromachining methods that have been implemented recently are listed in the following sections.

2.1 Silicon micromachining

Silicon micromachining has been employed to fabricate a patch antenna wherein, the silicon material was removed laterally underneath it thus producing a cavity that consists partly of air and partly of substrate (Papapolymerou et al., 1998, Hou et al., 2008, Ojefors et al., 2006, Kratz and Stenmark, 2005). Examples with both equal and unequal thicknesses of air and substrate have been implemented. The micromachined antenna configuration consisted of a rectangular patch centred over the cavity, sized according to the effective index of the cavity region, and fed by a microstrip line. To produce the mixed substrate cavity region, silicon micromachining was used to laterally remove the material from underneath the patch resulting in two separate dielectric regions of air and silicon. The amount of silicon removed varied from 50 to 80% of the original substrate thickness underneath the patch. A cavity model was used to estimate the effective refractive index value below the patch. The walls of the hollowed cavity tend to be, slanted owing to the anisotropic nature of the chemical etching, and this has to be allowed for in the modelling. This antenna has been shown to exhibit superior performance over conventional designs with the bandwidth and the efficiency having been increased by as much as 64% and 28%, respectively.

2.2 Polymer micromachining

Thick photoresist patterning processes can be used to fabricate an air suspended patch antenna either with supporting metallic posts or polymer posts. Antenna structures at

different frequency bands require different air cavity thickness to achieve optimum antenna performance and better impedance matching. Photoresist based polymers such as SU8 and THB151N can be used to obtain ultra thick supporting posts and can also be used as moulds for electroplating metal posts. Various polymer micromachining methods have been implemented in the past (Ryo-ji and Kuroki, 2007). A CPW fed post supported patch antenna has been fabricated on a Corning 7740 glass substrate which had a thickness of 800 μm and a dielectric constant of 4.6. Copper was used for metallization. The feed line of the antenna was patterned with the thick photoresist of AZ9260 and a two-step coating process was performed to form the posts of the antenna with a thick photoresist of THB151N. A simulated antenna gain in the range of 5.6 dBi to 9.0 dBi and the radiation efficiency varying from 92.8 % to 97.4 % were demonstrated for single patch antennas. In the case of a 2×1 array patch antenna, the simulated antenna gain and the radiation efficiency were from 5.8 dBi to 11.2 dBi and from 93.6 % to 95.3 %, respectively.

SU8, a widely used negative tone photoresist, has been used to fabricate an elevated patch antenna with micromachined posts of around 800 μm of height. (Pan et al., 2006; Bo et al., 2005) have successfully demonstrated an air-lifted patch antenna fabricated using surface micromachining technology. Both metal posts and polymer posts were used to provide mechanical support, as well as electrical excitation. A -10 dB bandwidth of 7%, centred at 25 GHz, was obtained. The proposed structure is superior to the conventional patch in terms of bandwidth, efficiency and lower side lobe level. While the traditional patch antenna directly printed on substrate usually gives a 3%-5% bandwidth and 70%-80% radiation efficiency, the proposed elevated patch will double the fractional bandwidth and gives a theoretical 97% radiation efficiency. This is achieved by eliminating the substrate loss. Low permittivity spin-on dielectric substrates are efficient for guiding microwaves and millimetre waves (Wang et al., 2005) and they have been used for microwave filters to improve the insertion loss of devices fabricated on silicon substrates (Leung et al., 2002).

2.3 Millimeter wave antennas using low permittivity dielectric substrates and micromachining

Antennas using low permittivity dielectric substrate have wider impedance bandwidth and higher gain when compared with those using ceramic dielectric substrates. Tong et al have presented the simulation and measurement of millimeter-wave CPAs (Coplanar patch antennas) using spin-on low-k dielectric substrate (Tong et al., 1995). The antenna composes of a gold ground plane at the bottom, two layers of BCB dielectric substrate ($\epsilon_r = 2.7$ and $\tan\delta = 0.002 @ 20\text{GHz}$) in the middle and a CPA pattern on the top. The total thickness of the BCB layer is 30 μm . Fluid state BCB is spun onto a 3-inch ground plane coated silicon wafer. The deposition technique is similar to the commonly used photoresist coating technique and the metal CPA pattern is evaporated onto the BCB dielectric layer. The thicknesses of the ground plane and the CPA pattern are both about 1.5 μm . The simulated and measured impedance bandwidths are about 1.2% and 2.6% respectively. The measured resonant frequency of the antenna is 38.3 GHz. Micromachining techniques employing closely spaced holes have been used underneath a microstrip antenna on a high dielectric-constant substrate to synthesize a localized low dielectric-constant environment ($\epsilon_r = 2.3$) (Gauthier et al., 1997). The holes are drilled using a numerically controlled machine (NCM) and extend at least 3.5 mm from the edge of the antenna in all directions and occupy the full substrate

height. The measured radiation efficiency of a microstrip antenna on a micromachined substrate (Duroid 6010, $\epsilon_r = 10.8$) increased from 48.3% to 73.3% at 12.8 - 13.0 GHz (including the loss with a 3.3 cm long feed line).

2.4 Integrated chip-size antennas using laser micromachining

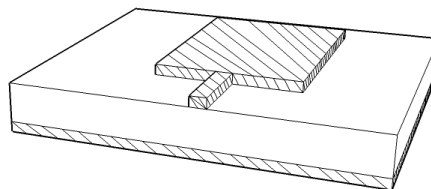
Integrated laser micromachined antennas on glass substrates are compact due to reduced size and owing to the relatively high dielectric constant. Mendes et al have reported an on-chip integrated, folded short-patch antenna (Mendes et al., 2006). It consists of three horizontal metal sheets that are electrically connected by two vertical metal walls. All this is embedded in a glass substrate having defined electrical permittivity and dielectric losses. The antenna was designed to operate at 5.1 GHz, a frequency chosen to be inside the 5 - 6 GHz ISM band. The fabricated antenna has dimensions of 4mm×4mm×1mm, a measured operating frequency of 5.05 GHz with a bandwidth of 200 MHz at the return loss of -10 dB and a simulated radiation efficiency of 60%. A method of applying laser micromachining technologies to fabricate a compact, high performance and low-cost 3D monopole antenna was proposed by Huang et al (Huang et al., 2005). The coplanar waveguide (CPW) fed configuration was used owing to its simple structure, wide bandwidth, and the ability of multi-band operation.

2.5 LTCC micromachining

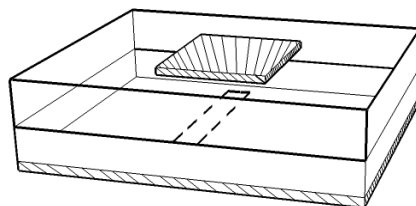
LTCC multilayer technology can be used to build up antenna arrays because it provides the necessary degree of vertical integration for the high-density microwave circuit and a packaging solution such as SIP (System in Package) (Wolff, 2007, Baras and Jacob, 2008, Wi et al., 2007). To optimise the material properties by reducing the relative permittivity of LTCC, a material modulation procedure based on punching air holes into the substrate is performed. Thereby, the relative permittivity of the material is replaced by the effective relative permittivity ϵ_r of the modulated material (Schuler et al., 2003).

3. Antenna design and modelling

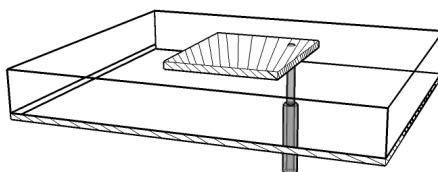
A compact planar antenna which is eminently suitable for embedding within integrated electronic systems is the patch antenna shown in Fig. 1. This type of antenna can be excited in one of four ways (Pozar, 1992, James and Hall, 1989, Bahl and Bhartia, 1980): (a) directly from a microstrip line, (b) electromagnetically from a buried line, (c) directly from a coaxial line probe, and (d) electromagnetically by means of a slot. Of these only (d) permits the implementation of multi-layered formats and consequently the section is directed toward assessing this geometry in relation to the micromachining of such structures.



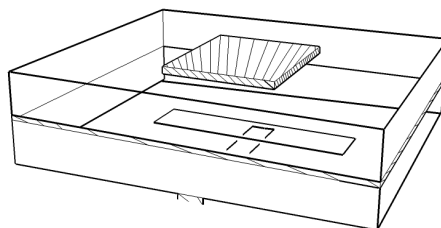
(a) Microstrip feed



(b) Buried line feed



(c) Coaxial feed



(d) Aperture coupled feed

Fig. 1. Illustration of feeding methods for microstrip antennas.

High gain and wideband micromachined microstrip and aperture fed stacked patch antenna devices have been designed and are described in the following sections. The antenna devices have been modelled using an electromagnetic simulation package. The structures are fabricated in layers and then assembled to obtain 3D devices. The detailed fabrication and assembly processes will be described. These aperture coupled devices are impedance matched for wideband operation. RF measurements show high gain and wideband operation for the devices and the results are in good agreement with that of simulation. The gain and bandwidth are determined to be 7.8 dBi and ~40% for a microstrip fed antenna device while they are 7.6 dBi and 38% for a CPW fed device.

3.1 Introduction to aperture coupled patch antenna

The design of microstrip antennas at microwave and millimeter wave frequencies is closely related to the feeding technique. At these frequencies, there are several problems such as feed dimensions, soldering of probes associated with the classical feeding techniques, such as coaxial probe (Fig 1 (c)) or edge feeds (Fig. 1 (a) and (b)). These considerations are even

more important for wideband applications, which require thicker substrates. On the other hand, the aperture coupled feeding technique (Fig. 1 (d)) has intrinsic properties which make it an attractive feature for millimeter wave applications. Wide-band operation of this type of microstrip fed antenna has been demonstrated at microwave and millimetre wave frequencies using either single or stacked patch configurations. Although all of the coupling methods depicted in Fig.1 have been shown to give excellent bandwidth characteristics, the indirect methods (Fig. 1 (b) and (d)) give rise to a high back-radiation level. However this is only true for aperture coupling (Fig. 1 (d)) if the aperture is near resonance. The aperture coupled antenna can also be fed with a CPW feed and is ideal at millimeter wave frequencies in the 30 GHz range (Mestdagh et al, 2004). It has been found that these antennas can easily be impedance-matched by tuning the dimensions of the excitation aperture and adding a small tuning stub.

Numerous advantages accrue for an aperture coupled configuration including those summarized previously (Pozar, 1985). They are listed below:

- (i) The configuration is suited for monolithic phased arrays, where active devices can be integrated on, for example, a gallium arsenide substrate with the feed network, and the radiating elements located on an adjacent (low dielectric constant) substrate, and coupled to the feed network through apertures in the ground plane separating the two substrates. The use of two substrates avoids the deleterious effect of a high-dielectric-constant substrate on the bandwidth and scan performance of a printed antenna array.
- (ii) No radiation from the feed network can interfere with the main radiation pattern, as the ground plane separates the two mechanisms.
- (iii) No direct connection is made to the antenna elements, so problems such as large probe self reactances or wide microstripline (relative to patch size), which are critical at millimetre-wave frequencies, are avoided.
- (iv) Ideal for micromachined antennas. The fabrication of a directly coupled feed probe would involve many fabrication steps.
- (v) The aperture coupled feeding technique has intrinsic properties which make it an attractive feature for millimeter wave applications.
- (vi) Wide-band operation of this type of microstrip antenna has been demonstrated at microwave frequencies (1 - 10 GHz) using either single or stacked patch configurations.
- (vii) A simple aperture coupled antenna structure gives rise to a high back-radiation level if the aperture is near resonance - this problem is eliminated by adopting a stacked antenna configuration.

A simple configuration of an aperture coupled microstrip antenna is shown in Fig. 1(d). It consists of a radiating patch on one substrate coupled to a microstripline feed on another parallel substrate, through an aperture in the intervening ground plane. It should be noted that the aperture coupled microstrip antenna can be used for both linear and circular polarizations. It requires two co-located orthogonal apertures each one excited by a different feed line. Each aperture excites orthogonal linearly polarized resonances under the normally square patch. The polarisation of the radiation from the patch is then dependent on the relative magnitude and relative phase of the signals entering the independent feed lines.

Circular polarisation is obtained when the signals are equal in magnitude and in quadrature phase.

For conventionally fed patch antennas (Fig. 1 (a) to (c)) it is well known that to a very good approximation the patch resonant frequency is dictated largely by the size and shape of the patch. This is not the case in aperture coupled patches. The aperture also has a resonant frequency and the coupled resonators formed by the aperture and the patch resonates at a frequency determined by simple filter theory. In this section a micromachined microstrip fed aperture coupled antenna is studied in depth. We then examine micromachined aperture coupled stacked antenna devices fed both from microstrip and CPW line. Antenna performances are assessed for various antenna configurations. Reflection coefficient (S_{11}), VSWR, normalise radiation pattern, gain, directivity and efficiency parameters are presented for a range of design parameters with the results plotted as a function of frequency as necessary. The effects of these different design parameters on the antenna performance are discussed.

3.2 Micromachined aperture coupled patch antenna

The gain and bandwidth of an aperture coupled antenna device can be significantly improved by introducing a micromachined air gap below the patch (see Fig. 2). These aperture coupled antenna devices which are described in ensuing sections are produced on a microwave PCB substrate. The air gap is achieved by suspending the patch on a micromachined polymer ring structure. A brief introduction to an established analytical design method is provided in order to communicate the fundamental operating principle of an aperture coupled antenna of the type described here. However, an electromagnetic field full-wave simulation software package is employed to design the antenna devices and adjust them for optimum performance. The effects of the design parameters, such as substrate material, air gap thickness, polymer rim dimensions and conductor materials, on the antenna's electromagnetic behaviour are investigated. The performances of several micromachined antenna devices are compared. Microstrip fed, CPW fed, single and stacked antenna configurations are included.

An aperture coupled antenna structure can be effectively modelled by means of a range of well established techniques. These are:

- Transmission line model (TLM)
- Finite element model (FEM)
- Finite difference time domain technique (FDTD)
- Method of moments technique (MOM)

All of these techniques exist in commercial packages. The general purpose modelling package, ANSOFT HFSS, is based on the finite element method, while CST Microstrips is based on the transmission-line matrix (TLM) method in time domain form. The IE3D package employs the method of moments. All are suitable for the kind of micromachined antenna devices described in this chapter. The antennas presented here are all modelled and optimised in the ANSOFT HFSS design environment.

The micromachined cavity-backed patch antenna design, realized by means of a polymer spacer, is quite similar to the strip-slot-form-inverted patch (SSFIP) antenna (Zürcher, 1988).

Fig. 2 shows a schematic of the cross-sectional and the top views of this potentially high gain, wide band antenna device. A square polymer ring (SU8 rim) mimics a sealed air filled cavity between the substrate and the polyimide thin film. The cavity-backed aperture coupled configuration improves radiation efficiency and thereby the gain of the antenna device. The configuration also improves the bandwidth of the antenna device owing to the proximity of the resonances of the coupling aperture and the patch.

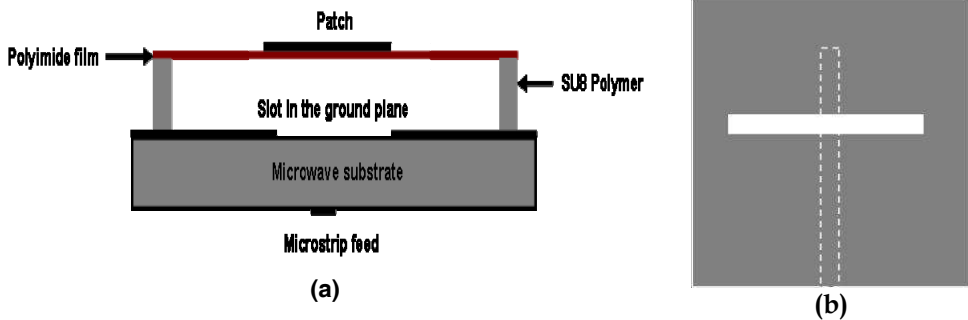


Fig. 2. Geometry of the (a) cross-sectional view and (b) top view of single patch micromachined aperture coupled antenna device.

The antenna centre frequency depends primarily on the dimensions of the resonant patch element and is given by

$$f_0 = \frac{c}{2L_{eff} \sqrt{\epsilon_{eff}}} \quad (1)$$

where f_0 is the centre frequency of the antenna, c is the speed of light, L_{eff} is the effective length of the patch element and ϵ_{eff} is the effective dielectric constant. The device was designed to operate at around 12 GHz for ease of characterization using in-house measurement facilities. The design parameters such as the dimensions of the microstrip feed, aperture and top patch were optimized using the Ansoft HFSS electromagnetic simulation package with the aim of achieving high antenna radiation efficiency.

Parameter	Unit (mm)
Patch length	9.5
Patch width	11.5
Patch thickness	0.007
Slot length	11
Slot width	1.1
Microstrip length	18.84
Microstrip width	0.85
Inner length of cavity	19
Inner width of cavity	19
Cavity height	1.5
Thickness of polyimide film	0.125
Thickness of microwave PCB substrate	1.51

Table 1. Summary of the design parameters for the microstrip fed suspended patch antenna.

The height of the polymer rim was adjusted to obtain high gain. In the HFSS simulation, the lateral dimensions of the polymer rim were chosen to achieve high efficiency and compact size for the antenna structure. Table 1 summarizes the design parameters of the antenna device. A microwave PTFE material, AD300A, from Arlon MED (<http://www.ctsind.com.sg/arlon.html>), was used as the base substrate while a polyimide thin film (Du Pont) provided the supporting substrate for the suspended patch. The dielectric constant and loss tangent of the PTFE substrate are respectively 3 and 0.003. For the SU8 rim material they are 4.2 (Thorpe et al., 1998) and 0.042 (Lucyszyn, 2001) respectively, while the corresponding values for polyimide substrate material are 3.5 and 0.0026. In order to accurately model the performance of the antenna device, the parasitic effects of the SMA connector are simulated by introducing a short and wide rectangular extension at the input of the microstrip feed line. The dimensions (3mmx1.5mm) of the extension are chosen to match the length and diameter of the pin of the SMA connector. It has been observed that accommodating the effect of the connector is vital in order to accurately model the reflection characteristics of the suspended patch antenna. In the following sections the S_{11} parameters for estimating the bandwidth, normalised radiation pattern and radiation efficiency obtained from the HFSS designer environment are presented and discussed.

3.2.1 S parameters and study of the bandwidth

To assess the performance of the micromachined aperture coupled antenna device shown in Fig.2, the return loss (reflection coefficient in dB) and VSWR (voltage standing wave ratio) parameters are plotted for an optimum antenna, as in Fig. 3.

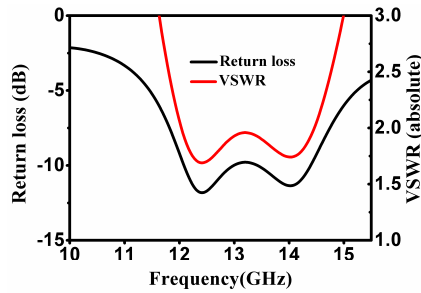


Fig. 3. Simulated return loss and the VSWR parameters for the optimized micromachined aperture coupled antenna device.

The return loss and VSWR parameters are plotted as a function of frequency from 10 to 15.5 GHz. It can be seen from the plot that the return loss is lower than -10 dB from around 12 GHz to 14.3 GHz and the VSWR is lower than a value of 2 in this range. Therefore the corresponding theoretical bandwidth of the antenna is 2.3 GHz or 17%.

3.2.2 3D antenna radiation pattern

The radiation pattern for the antenna device is obtained from the electromagnetic field solution and is plotted as a function of frequency from the far field plotter interface in Ansoft HFSS. Figure 4 shows the 2D and 3D far-field radiation patterns for the aperture coupled antenna device at 13.2 GHz near to the centre frequency of the operating band. The patterns show that there is high backward radiation and obvious side lobes in the E plane. But it will be shown in the later sections that the side lobes and back side radiation are reduced significantly using stacked patch configurations.

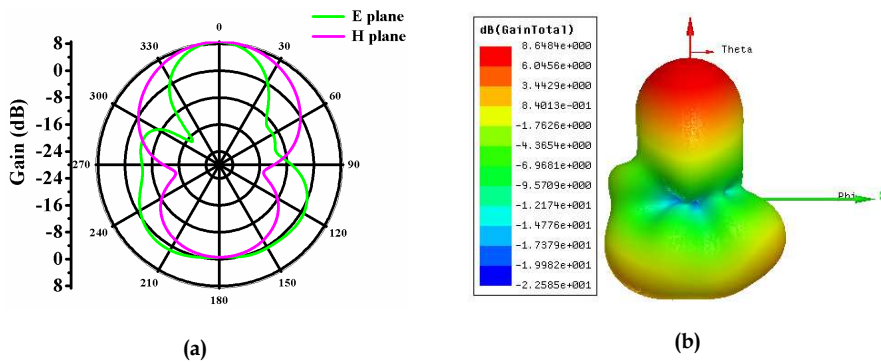


Fig. 4. 2D (a) and 3D (b) radiation patterns of a microstrip fed single patch antenna device at 13.2 GHz.

3.2.3 Directivity and gain

Fig.5 shows the variation of directivity, gain and efficiency for the microstrip fed aperture coupled antenna device with respect to frequency from 10 GHz to 15.5 GHz. The left 'y' axis gives the magnitude of antenna directivity and gain while the right 'y' axis gives the magnitude of absolute efficiency from 0.9 to 1. It can be easily seen from the plot the gain curve follows the directivity curve suggesting almost 100% radiation efficiency within the radiation bandwidth region. The gain varies from about 5 dBi at 10 GHz to around 8.3 dBi at 13 GHz and falls back below 6 dBi after 15.5 GHz. The excursions of directivity and gain within the radiation bandwidth (12 - 14.3 GHz) are below 1 dBi while it varies very significantly outside of this frequency range. The radiation efficiency varies from about 0.95 to close to 1 at 15.5 GHz. It should be noted that the radiation efficiency is a measure of total loss, including dielectric and conductor losses, within the micromachined antenna structure and it improves dramatically with the introduction of the micromachined air cavity.

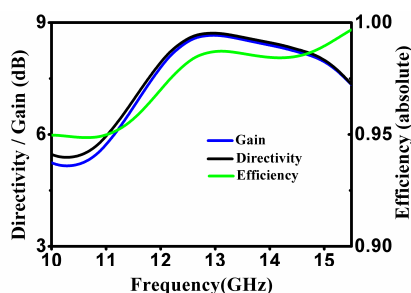


Fig. 5. Simulated gain, directivity and radiation efficiency for the optimized micromachined antenna device.

3.3 Stacked patch antenna devices

The design and modelling of the microstrip and CPW fed, stacked aperture coupled antenna devices is presented in the following sections. These stacked antenna devices are designed using a similar micromachined aperture coupled model as that presented in section 3.2. The stacked antenna configuration is exploited to further enhance the bandwidth and radiation pattern. The bandwidth is improved by utilizing the multiple closely resonant structures as well as through better impedance matching with the lower patch elements in the stacked configuration. The stacked patch elements are fabricated on polyimide substrates for microstrip fed devices and on LCP (liquid crystal polymer) film substrates for the CPW configurations, supported, in all cases, by the micromachined SU8 polymer spacers

3.3.1 Microstrip fed aperture coupled stacked patch antenna

3.3.1.1 Antenna Design

Stacked, cavity backed, aperture coupled antenna geometries have been modelled using Ansoft HFSS and optimized. Fig. 6(a) provides a cross sectional view of a microstrip fed stacked antenna of the type described in this section, while the top view of the coupling aperture on the lower microstrip substrate surface is depicted in Fig. 6(b). The arrangement consists of a double cladded microwave PTFE substrate, and two suspended patches to form

a stacked antenna device. The microstrip feed line on the bottom surface of the microwave substrate excites the lower patch through a rectangular coupling aperture in the ground plane which forms the top surface of the microwave substrate. The patch elements are printed on thin film (polyimide) substrates. They are supported by micromachined polymer spacers to reduce the antenna loss and hence to improve its gain. The cavities are sealed by the bonded polymer rings thus providing protection against the incursion of moisture and particles, which could contribute unwanted losses.

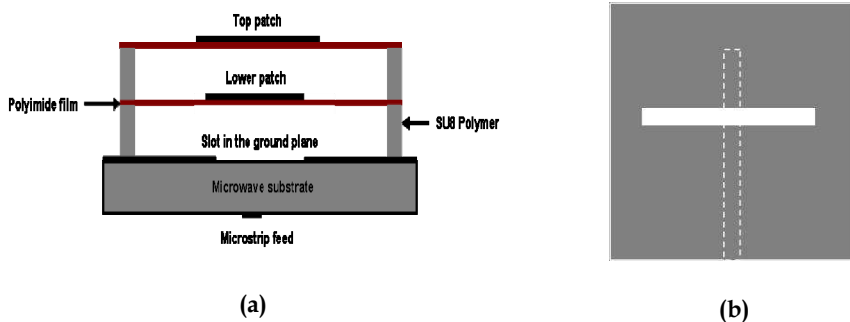


Fig. 6. (a) Schematic cross-sectional view of the stacked microstrip fed aperture coupled antenna using micromachined polymer spacers, (b) The top view of the aperture and feed line on the substrate surfaces.

Parameter	Microstrip fed device (mm)	CPW fed device (mm)
Lower patch length	5.8	9.4
Lower patch width	9	18
Upper patch length	9.6	12.6
Upper patch width	10.6	18
Patch thickness	0.009	0.009
Slot length	9.8	16.5
Slot width	0.98	1.6
Microstrip length	15.00	18.2
Microstrip width	0.82	1.4
Inner length of cavity	19	18.2
Inner width of cavity	19	18.2
Lower cavity height	2.2	1.0
Thickness of polymer rim	1.0	1.0
Upper cavity height	0.67	1.0

Table 2. Summary of the design parameters for the suspended stacked patch antennas

The stacked antenna has been designed using a similar approach to that described previously for the development of multi-layer stacked wideband antenna devices (Pavuluri et al., 2008, Wang and Pavuluri, 2008, Croq and Pozar, 1991). It is designed for operation at

X-band (8 – 12 GHz) with a 40% of bandwidth. The height of the air cavities formed by the micromachined polymer rims located between each stacked patch and the substrate, is adjusted for optimum bandwidth while at the same time maintaining a low profile for the overall antenna structure. For this microstrip fed device, the top patch and the aperture are dimensionally adjusted to ensure resonance at similar frequencies, while the dimensions of the microstrip line and the lower patch are tuned to secure the best possible impedance match. In the design process the initial dimensions of the patches are determined by the choice of the center frequency of operation. The width of the coupling aperture is conventionally set at about 10% of its length.

The heights of the air cavities as explained earlier are a trade-off between the desire for bandwidth and the limitations set by the fabrication process. The length of the feedline is then varied to obtain sufficient bandwidth. In order to obtain fixed band performance, the lengths of the top patch and the aperture are modified to tune the band of operation. Fine impedance tuning is achieved by adjusting the dimensions of the lower patch. The shape and dimensions of the SU8 spacer rings are chosen carefully to ensure good antenna performance. It is generally necessary to carry out several iterations of the above steps to obtain an acceptable antenna delivering high gain and wide bandwidth. The optimized design parameters are given in Table 2.

3.3.1.2 S parameters and study of the bandwidth

To determine the predicted performance of the optimally designed aperture coupled antenna, the return loss and VSWR are plotted as a function of frequency. The plot width at the -10 dB return loss locations as in Fig.7, quantifies the bandwidth. From the plot the return loss is lower than -10 dB from about 7.8 GHz to 12 GHz. The VSWR is lower than a value of 2 over this range. Therefore the theoretical bandwidth of this device is 4.2 GHz or 42%. This is an improvement of a factor of 2.5 over that of the single patch device.

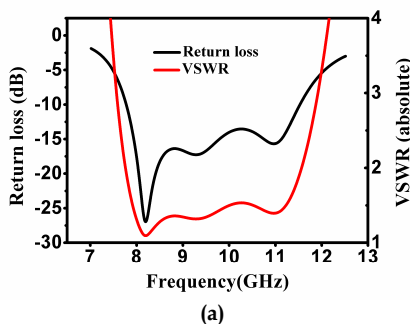


Fig. 7. Simulated insertion loss and VSWR parameters for the optimized micromachined microstrip fed stacked aperture coupled antenna.

3.3.1.3 3D antenna radiation pattern

The radiation pattern for the antenna device is obtained from the electromagnetic field solution and is plotted as a function of frequency using the far field plotter interface in Ansoft HFSS. Figure 8 shows the 2D and 3D far-field patterns for the aperture coupled

antenna device at 9.82 GHz near to the centre frequency (9.9 GHz) of the operating band. It can be seen that the back side radiation is reduced to around -4 dB for the microstrip fed stacked patch antenna configuration.

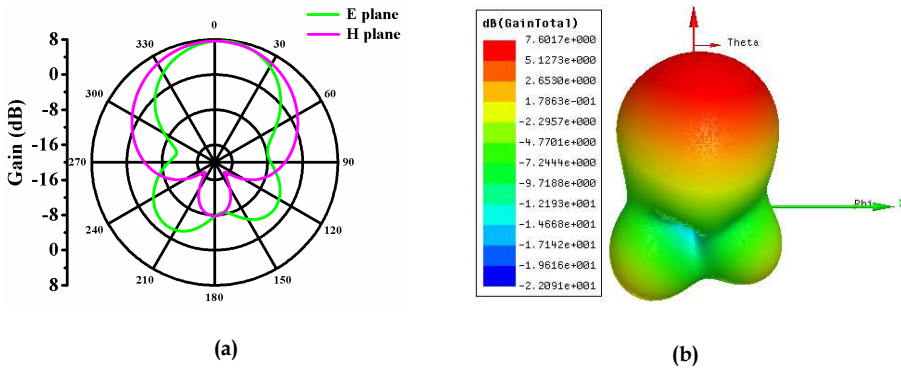


Fig. 8. 2D (a) and 3D (b) radiation patterns at 9.82 GHz.

3.3.1.4 Directivity and gain

Fig. 9 shows the dependence of directivity, gain and efficiency on frequency, in the range from 7 GHz to 12 GHz, for the microstrip fed stacked antenna. The results are not too dissimilar to those of the single patch antenna (Fig. 4), but with less gain and efficiency variation over the optimum operating band. The gain and directivity vary from about 6 dBi at 8 GHz to around 7.8 dBi at 9.7 GHz and falls back below 6 dBi after 12.5 GHz. The directivity and gain are constant to within 2 dBi over the previously defined -10dB bandwidth. Outside this bandwidth gain diminishes significantly. The radiation efficiency is greater than 0.95 from 8 GHz to 12 GHz.

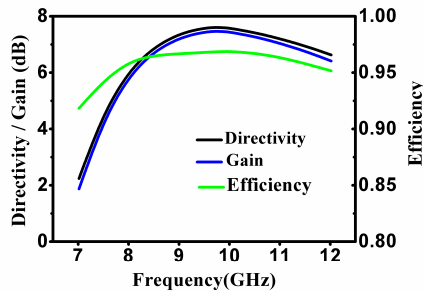


Fig. 9. Simulated gain, directivity and radiation efficiency of the optimized micromachined microstrip fed stacked aperture coupled antenna.

3.3.2 CPW-fed aperture coupled micromachined patch antenna

An antenna comprising three stacked patches fed from a coplanar waveguide (CPW) has also been studied. Fig. 10 show the schematics of the CPW fed stacked patch antenna. A single clad PTFE substrate (Taconic TLY-3-0200-CH/CH) was used to support the CPW line and the coupling aperture. The stacked patches are suspended symmetrically above the

aperture using micromachined SU8 polymer rims. As the air gap between the base microwave substrate (Fig. 10(a)) and the lowest patch is smaller than that of the microstrip fed stacked device (Fig. 6(a)) for ease of fabrication, an additional patch is required to yield a similar bandwidth of ~40%. The upper pair of patches has the same dimensions and it is the electromagnetic coupling between them that further increases the bandwidth of the antenna. The coupling slot on the ground plane and the top two patches were designed to be in close resonance. The bottom patch and the $\lambda/4$ stub are optimized for a wide ‘match’ bandwidth. Tables 2 and 3 show the physical dimensions of the structure layers for the antenna device.

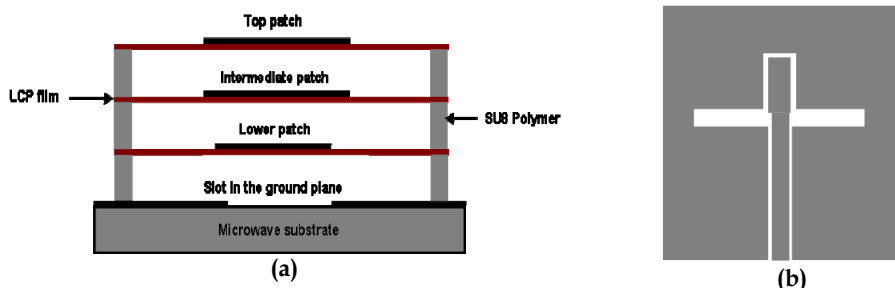


Fig. 10. (a) Cross-sectional view of the stacked CPW fed antenna using micromachined polymer spacers, (b) top view of the corresponding aperture and feed line on the substrate surface.

Substrate	Thickness (mm)	Dielectric constant	Loss tangent
Taconic PTFE substrate	0.5	2.2	0.0009
LCP film	0.10	3.2 (Thompson et al., 2004)	0.002

Table 3. The thickness and microwave property of Taconic PTFE and LCP substrates.

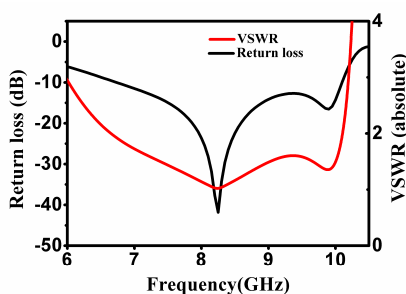


Fig. 11. Simulated insertion loss and VSWR parameters for the optimized micromachined CPW fed stacked aperture coupled antenna.

3.3.2.1 S parameters and study of the bandwidth

The return loss and VSWR parameters are plotted as a function of frequency from 6 to 10.5 GHz in Fig.11. It can be seen from the plot that the return loss is lower than -10 dB from

around 6.5 GHz to about 10.2 GHz, and the VSWR is lower than a value of 2 over this range. The corresponding theoretical bandwidth is 44%.

3.3.2.2 Radiation pattern and gain

As with earlier examples, the radiation pattern for the antenna device is obtained from the electromagnetic field solution. It is plotted at a given frequency using the far-field plotter interface in Ansoft HFSS. Fig. 12 shows the 2D and 3D far field patterns for the aperture coupled triple patch antenna device at 8.3 GHz. It can be seen that the back side radiation is reduced to around -7 dB in the E and H plane radiation characteristics. The backward radiation is significantly less than that of the microstrip fed devices. The reduction of the back radiation can be attributed to the effect of the CPW based feeding method. Thus the CPW feeding approach is recommended for minimal backward radiation.

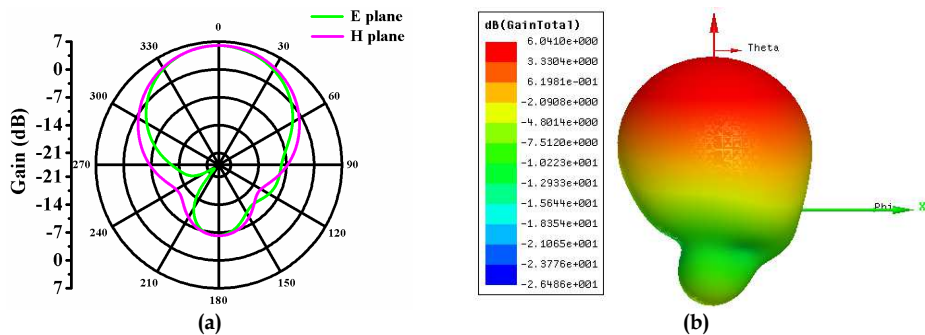


Fig. 12. 2D (a) and 3D (b) radiation patterns for the CPW fed stacked antenna at 8.3 GHz.

3.3.3 The effect of polymer rim design on the performance of the CPW fed stacked aperture coupled antenna

As stated previously the SU8 polymer has high dielectric loss at microwave frequencies with a loss tangent of 0.043. The effect of the dimensions of the polymer rim on antenna performance has been studied using the CPW fed antenna design. Two rim designs of 23mmx23mm and 12.5mmx18mm are used and the corresponding projected views of the antennas are shown in Fig. 13. The other design parameters remain the same as shown in Table 2. Fig. 14 shows the efficiency of the CPW fed stacked antenna device for the two polymer rim designs in the frequency range of 6.5 GHz to 10.5 GHz. As can be seen from Fig. 14 the efficiency of the antenna device for the larger rim is greater than 0.95 from 6.5 GHz to 10.5 GHz but it is less than 0.9 with the smaller polymer rim. It can also be seen that the roll-off rate of the antenna efficiency above 9.5 GHz is much faster for the smaller rim indicating rapid decrease of the antenna performance.

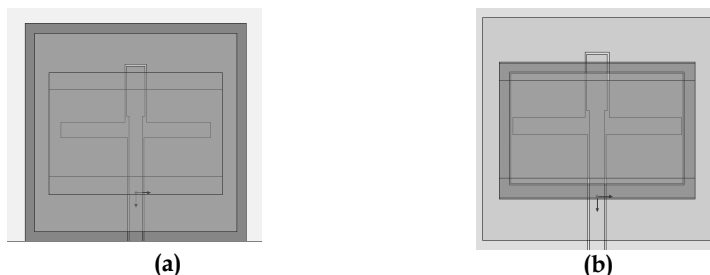


Fig. 13. A 3D view of the optimized micromachined CPW fed stacked aperture coupled antenna with two different polymer rim dimensions.

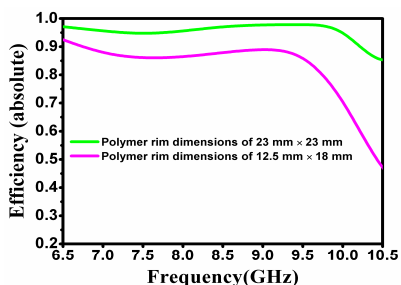


Fig. 14. Results of antenna efficiency of the CPW fed antenna for different SU8 polymer rim dimensions

3.3.4 Effect of the substrate loss

As the losses in the substrate layers in a stacked antenna affects its performance significantly, for comparison, FR4 and PTFE based stacked CPW antenna designs with similar dimensions as that of the CPW antenna shown in Fig. 10 are also designed and optimized for impedance matched performance. These two devices consist of 4 layers of FR4 or PTFE material with 3 three stacked patches. The dielectric constant and the loss tangent for the FR4 material are taken as 4.2 and 0.020 respectively (Aguilar et al., 1998). Fig. 15 shows the efficiency and gain as a function of frequency for the three CPW fed stacked antenna configurations. The rapid decrease of gain above 9 GHz of the FR4 based device is due to the increased insertion loss as the frequency is out of the band of operation. The gain of the antennas was obtained from the simulation results of the radiation characteristics. It can be seen that there is little difference between gain values of the stacked patch antenna based on the multilayer PTFE structure and the devices with suspended patch elements since the dielectric loss is minimal in both cases. However, the micromachined device has a larger bandwidth. The performance of the FR4 based multilayer antenna is much poorer due to the well known lossy behaviour of the FR4 material beyond the microwave frequency region. Table 4 gives a summary of the performance parameters. The micromachined antenna device with suspended patches showed the best bandwidth of about 38% close to that required for ultra-wide band applications.

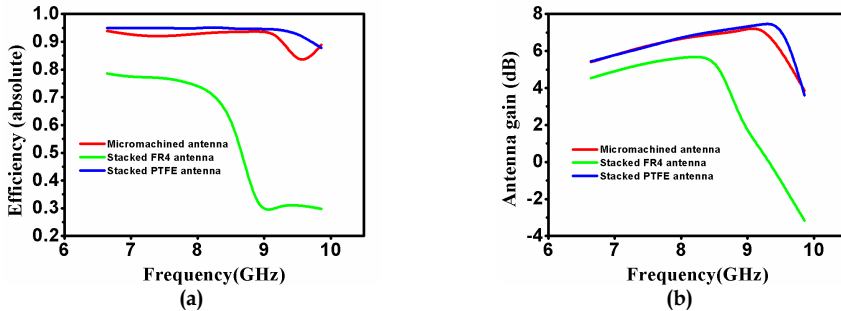


Fig. 15. (a) Results of antenna efficiency of the CPW fed stacked patch antenna for different substrate configurations, (b) the corresponding results for the gain of the devices.

CPW fed antenna design	Bandwidth (%)	Peak gain (dBi)	Efficiency (%)
Suspended patches on PTFE substrate	38.3	7.8	97.5
Stacked PTFE substrates	30.1	7.9	99
Stacked FR4 substrates	32.7	3.6	75

Table 4. Summary of performance parameters for different antenna configurations.

4. Fabrication and assembly

4.1 Overview of antenna fabrication and assembly

New fabrication and assembly methods have been developed to produce the antenna devices described in the previous sections. The antenna structures are fabricated in layers and then assembled using micromachined polymer spacers. Fig. 16 shows the schematic of the layers of a microstrip fed antenna with multiple patches to illustrate the low temperature assembly method. The feeding and coupling structures are produced on a PCB substrate using the conventional PCB technology or a microfabrication method for devices requiring high resolution metal line and aperture structures. The patches and the supporting micromachined polymer structures are fabricated on thin film polymer substrates. Polyimide and liquid crystal polymer thin films are suitable materials as the substrates for supporting the patches. After fabrication of the patch, the millimeter thick polymer structure for supporting the thin film substrate is fabricated using a surface micromachining method. An additional polymer spacer can be fabricated on the PCB substrate in order to produce a larger air gap between it and the polymer substrate about it. In this case the two spacers should be matched. The layers of the antenna are then aligned and bonded together to produce a stacked patch antenna device.

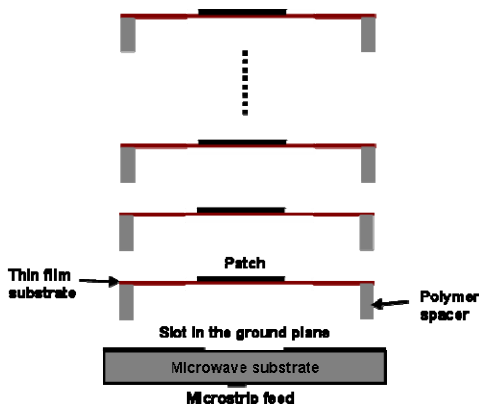


Fig. 16. Illustration of the assembly method for construction of a generalized micromachined antenna device.

4.2 Fabrication of antenna layers

All of the antenna layers are fabricated using microfabrication methods though some of the antenna structures such as the patches can be fabricated using the conventional PCB technology. A MEMS based fabrication process has been implemented to obtain precision metal patterns on the substrates with the aim of reducing metal losses at higher frequencies. In general, the fabrication process outlined in the following sections can be implemented with different substrate materials as long as the thermal stress due to the CTE (coefficient of thermal expansion) mismatch between the SU8 polymer and the substrates can be accommodated without the risk of the delamination of the SU8 structures from the substrates. In addition, this fabrication process can be used for constructing other passive devices such as high performance filters at millimetre wave and terahertz frequency regimes.

4.2.1 Substrate fabrication

Commercial microwave PCB substrates (Arlon MED300) are used as the base substrate for the microstrip fed antenna devices described in the previous section. The microstrip and the coupling aperture are fabricated using the copper cladding layers on the substrate. Fig. 17 shows the schematic of the fabrication steps. After cleaning and drying, both sides of the substrate are deposited with a photoresist layer (AZ9260, Clariant). The photoresist layers are deposited by spin coating and the thickness is about 10 μm . After deposition, the substrate wafer is left at room temperature for a few minutes to allow the air bubbles trapped in the resist film to propagate to the surface to eliminate the formation of defects in the photoresist layer after baking. In the photolithographic process the photoresist layer is exposed to UV light on a mask aligner using a high resolution polymer photomask to define a pattern for the microstrip line.

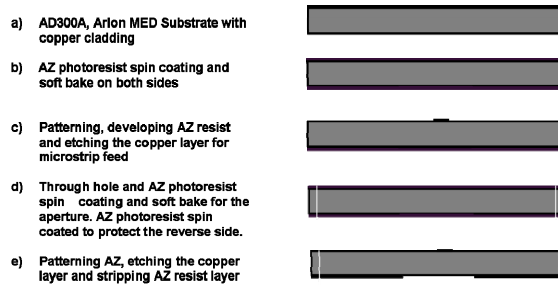


Fig. 17. Process flow of substrate fabrication for the microstrip fed antenna device.

The photoresist layer is then developed and the exposed copper is etched in a ferric chloride based etching bath. Careful control is necessary to ensure a well defined microstrip line. The photoresist layer is removed to complete the fabrication process for the microstrip line. For alignment of the microstrip to the aperture to be fabricated on the opposite side of the substrate in the subsequent fabrication process, precision holes are drilled at the corners of the substrate using a mechanical drilling method. Then both sides of the substrate are coated with a photoresist layer for fabrication of the coupling aperture and protection of the microstrip line. The same photoresist patterning and metal etching processes as for the microstrip are repeated to obtain the aperture. Fig. 18 shows the images of the fabricated microstrip line and aperture on the substrate. In the substrate fabrication process for the CPW fed device using PTFE substrates from Taconic only single sided metal patterning is required to fabricate the CPW structures.



Fig. 18. Optical images of (a) a feeding microstrip and (b) a coupling aperture on a substrate after fabrication.

4.2.2 Fabrication of patches on thin film substrates

Polyimide and LCP (liquid crystal polymer) based films are used as the thin substrates for the suspended patches. The thicknesses of the polymer films are 125 μm and 100 μm respectively. These substrate materials are low-cost and are well known for the excellent dielectric, thermal and mechanical properties for microwave applications. As the film substrates do not have a copper cladding layer, a copper foil of 9 μm from Taconic is laminated on the substrate for patch fabrication. Alternatively the patch can be fabricated using electrodeposition of copper.

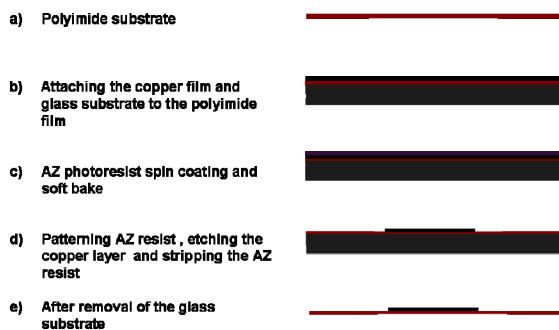


Fig. 19. Fabrication flow for the suspended patches.

In both cases the patch is defined by the photolithography method. As the thin film polymer substrate is flexible it is attached to a glass wafer for easy handling during patch fabrication. Fig. 19 illustrates the schematic of the process flow for patch fabrication on the polymer substrate following the lamination of the copper foil. A layer of photoresist is deposited on the substrate by spin coating and is then patterned by photolithography to define the patch structure. Following copper etching and photoresist stripping a patch is obtained on the thin film substrate. Several patches can be fabricated on a polymer film. The alignment marks are fabricated at the same time as for the patches.

4.2.3 Fabrication of micromachined spacers

The millimetre thick polymer spacer rims are fabricated on the thin film substrates after patch fabrication using the polymer surface machining method. Polymer micromachining is a process where high aspect ratio polymer structures are fabricated out of a thick polymer film on a substrate. We have used the photo-imageable SU8 epoxy polymer to produce the polymer structures on the substrate layers for constructing the antenna devices described in the previous section. The SU8 polymer is a well known micromachining material for MEMS applications. It is a low cost material, easy to deposit in thick films by spin coating or spreading, low processing temperature (~110°C) and chemically inert. A wide range of film thicknesses from microns to millimetres can be obtained by modifying the composition of the chemical formulations for film deposition. The thick film and high aspect ratio capabilities have made the SU8 polymer an ideal material for the spacer rims for the antenna devices. The SU-100 polymer solution was prepared and used in order to fabricate millimeter thick polymer spacers. The composition of the solution is given in Table 6. Fig. 20 shows the process flow for fabrication of SU8 spacer rims on the substrate layers for antenna assembly. The required spacer thickness for each antenna layer is obtained by controlling the spin speed and time in the deposition of the SU8 layer.

Composition	Percentage
SU8 resin	72.9%
Gamma-butyrolactone liquid	21.1%
Photoinitiator	6%

Table 6. The composition of the SU8-100 solution.

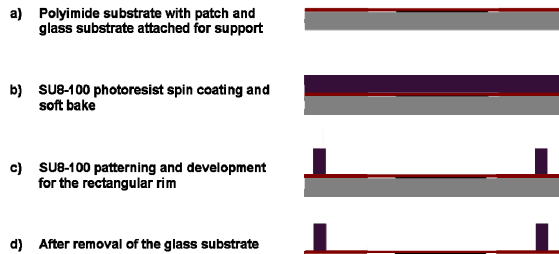


Fig. 20. Fabrication flow for the SU8 polymer rim.

After soft baking the film is exposed to the i-line (365 nm) of the UV source on a mask aligner using the photomask with the patterns of the spacer rims. The SU-8 layer is heated to 65°C on a hotplate for post exposure bake. Then the SU8 layer is developed in the EC solvent to remove the unexposed SU8 in the photolithography process. Mild agitation provided by a magnetic stirrer can be used to reduce the development time and improve the quality of the resultant SU8 structures.

In order to create the large air gap between the microwave substrate and the suspended patch above it for the microstrip fed devices it is useful to fabricate two matching spacer rims one on each of the microwave and the film substrates. Fabrication of the millimetre thick SU8 spacer rims on the rigid Arlon MED substrate is more challenging than the thin film substrates and an optimized process for soft baking is necessary. Otherwise delamination of the SU8 spacer rims from the substrate occurs after the fabrication process due to the higher interfacial stress built up in the baking process prior to photolithography. The increased stress is caused by the larger CTE mismatch between the SU8 layer and the rigid microwave PCB substrate than the film substrate. However this problem can be solved by careful control of the temperature profile in the soft baking process, a smooth temperature profile in the heating and cooling processes is required (Patel et al., 2008). As a result millimetre thick SU8 polymer rims on microwave substrates are successfully fabricated.

4.3 Antenna assembly

The fabricated substrate layers are assembled using a low temperature polymer bonding process to form high performance antenna devices. This is a new method for creating antenna devices with suspended patch elements. Fig. 21 illustrates the process steps for assembly of a microstrip fed stacked patch antenna. A thin layer of SU8-100 solution is

applied to the top surface of the polymer rims as the bonding material for antenna assembly. The polyimide film supporting the lower patch is attached to the substrate by bonding of the SU8 rim on the polyimide film to the corresponding one on the base substrate. Then the polyimide film with the top patch was attached to the polyimide substrate of the lower patch by bonding the SU8 rim to the polyimide film. Precision alignment marks on the polyimide films and the base substrate were used to facilitate the accurate alignment of the layers. The bonding process can be carried out on a hotplate or on a flip chip bonder.

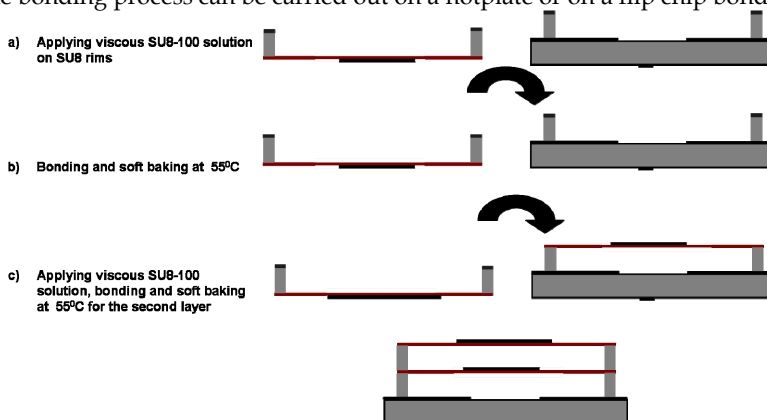


Fig. 21. Process flow for the antenna assembly.

The polymer rim on the lower surface of the polyimide substrate is aligned and attached to the rim on the microwave substrate. The assembly is heated to 55°C and maintained at this temperature for 10 minutes for bonding the two polymer rims together. The thin film substrate with the top patch is then assembled on top of the substrate layer with the lower patch using the same bonding approach. After the assembly process a stacked patch antenna device was obtained. For RF characterization to evaluate the performance of the device, an SMA connector was attached to microstrip and ground plane on the microwave substrate. CPW fed antennas are assembled using the same method Fig. 22 shows the images of the assembled antenna devices. For the CPW fed device, the patches are on the bottom surface of the LCP substrates. The most critical parameters determining the quality of the bonding are the thickness uniformity of the SU-8 rims, the amount of SU8-100 solution applied to the surface of the SU8 rims and the bonding pressure and temperature. SU8 rims with good surface uniformity can be obtained using an optimized fabrication process. The amount of liquid SU8-100 for bonding is determined by minimizing void formation and at the same time reducing the overflow of the material during bonding. A good bonding temperature is 65°C which is just above the glass transition temperature (64°C) of the SU8 material but not high enough to cause significant overflow as the viscosity changes rapidly around the glass temperature (Tuomikoski and Franssila, 2005).



Fig. 22. Optical images of the assembled stacked antennas (a) microstrip fed and (b) CPW fed device.

5. RF Measurements

In the following section, the RF measurements for S_{11} parameters and the radiation patterns along with the results of gain measurements are presented and compared with the Ansoft HFSS simulation results. The S_{11} parameters are obtained from a HP 8510 network analyzer after calibrating the coaxial cables. Radiation patterns are obtained by measuring the S_{21} parameters between the AUT (Antenna Under Test) and a reference 20 dBi standard gain horn in X band. The three antenna gain measurement technique was used for the micromachined aperture coupled single patch antenna device while a gain comparison technique was used for the stacked antenna configurations. The antenna measurements were conducted in an $8\text{m}\times 3\text{m}\times 3\text{m}$ anechoic chamber with a separation distance of 1.5 m between the reference and the AUT.

5.1 Results of reflection measurements

Fig. 23 shows the measured and simulated results of S_{11} for the single patch aperture coupled antenna device. The resonance at 14.2 GHz is that of the patch while the one at 12.1 GHz is associated with the slot. The -10dB bandwidth of the device was determined to be 19% from the measured results, a factor of 2 larger than that of the probe fed, post supported device (Pan et al, 2006).

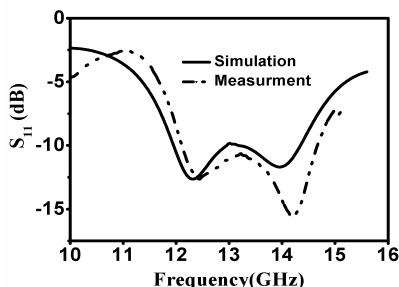


Fig. 23. Simulation and measurement results of the reflection characteristic of the high gain aperture coupled patch antenna.

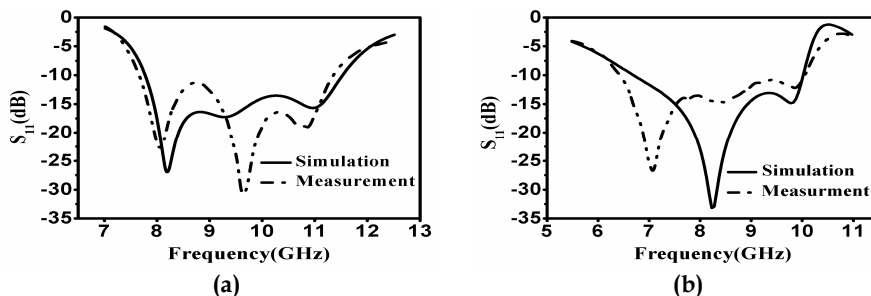


Fig. 24. Simulation and measurement results of the reflection characteristics for the high gain wideband stacked antennas, (a) microstrip fed device and (b) CPW design.

Fig. 24 shows the measured and simulated results of the reflection characteristic (S_{11}) of the microstrip fed and CPW fed stacked antenna devices. The -10dB bandwidth for the microstrip fed stacked patch antenna device is determined to be 3.9 GHz or 40% from the measured results. The corresponding result for the CPW fed stacked patch antenna is 3.25 GHz or 38%. It can be seen that the measured results agree well with that of the simulation apart from the downward frequency shift. This shift, particularly in the vicinity of the main resonance, can be attributed to the effect of the SMA connector overlay which was not included in the simulation.

5.2 Results of radiation measurements

Fig. 25 shows the gain-factor results for the micromachined single patch antenna device measured at 12.1 GHz. The gain of the antenna is about 8.3 dBi. Figs. 26 and 27 show the measurement and simulation results of the normalized radiation pattern for the stacked antenna devices. The maximum gain of the microstrip fed antenna devices is about 7.8 dBi at ~10.5 GHz while the maximum gain of CPW fed antenna device is about 7.6 dBi at ~10 GHz. The results show good agreement between measurement and simulation.

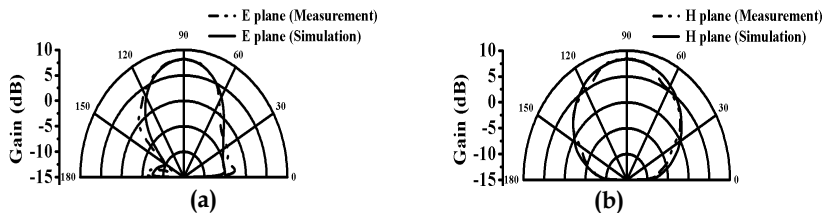


Fig. 25. Simulated and measured E-plane (a) and H-plane (b) radiation patterns for the microstrip fed single patch antenna device at 12.1 GHz.

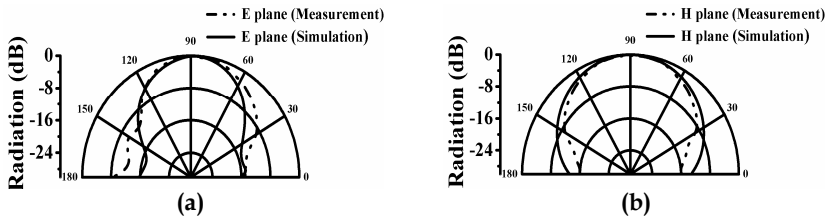


Fig. 26 Simulated and measured E-plane (a) and H-plane (b) radiation patterns for the microstrip fed antenna device at 10.5 GHz.

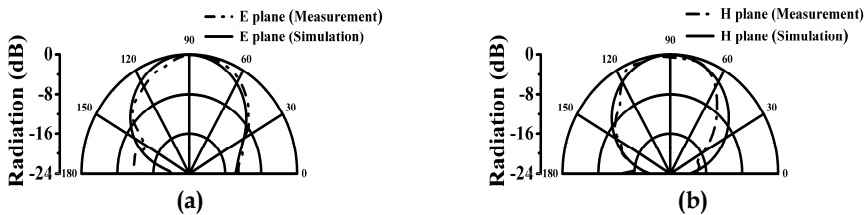


Fig. 27. Simulated and measured E-plane (a) and H-plane (b) radiation patterns for the CPW fed antenna device at 10 GHz.

6. Conclusions

Micromachined aperture coupled patch antenna devices have been developed using polymer micromachining and micro-assembly methods. The antennas are fabricated in layers and then assembled using micromachined polymer spacers and a low temperature polymer bonding method. By creating air cavities between the radiating patches and the substrates using polymer rims, the efficiency, gain and bandwidth of the devices have been improved significantly over conventional microstrip patch antennas. The potential radiation efficiency of the devices is as high as 98% based on the simulation results. The wideband operation is achieved by employing several controls. These are: optimally tuning resonances associated with the antenna device; through the use of stacked patches as impedance transformers by optimizing the dimensions of the lower patches; by adjusting the tuning stub and the input aperture dimensions. This polymer based stacked antenna process has a dual function of supporting the air suspended radiating patches and for antenna module packaging. The new fabrication method provides an alternative low cost packaging approach as compared to conventional LTCC and PCB technology. The suspended patch antennas are lightweight and can be fabricated easily using polymer micromachining and bonding approaches. Similar devices can be designed for other frequency bands to meet the requirements of potential applications in the emerging field of UWB networks, WLAN networks at 60 GHz and automotive collision radar. The fabrication method could be developed into an effective packaging technology for millimetre wave and terahertz based sensor and communication systems. Antenna array devices can also be fabricated for high gain wideband applications.

7. References

- AGUILAR, J. R., BEADLE, M., THOMPSON, P. T. & SHELLEY, M. W. (1998). The microwave and RF characteristics of FR4 substrates. *Proceedings of the IEE Colloquium on Low Cost Antenna Technology (Ref. No. 1998/206)*, pp. 2/1-2/6, London, 24 Feb. 1998.
- Arlon materials for electronics (MED), orlando, florida, ([Online]. Available: <http://www.ctsind.com.sg/arlon.html>), Data sheet for AD 300A PTFE. (woven fiberglass/ micro-ceramic filled laminate for RF & microwave printed circuit boards).
- BAHL, I. J. & BHARTIA, P. (1980). *Microstrip Antennas*, Artech House, ISBN 978-0890060988, Dedham, Massachusetts.
- BARAS T. & JACOB, A. F. (2008). Manufacturing reliability of LTCC millimeter-wave passive components. *IEEE Transactions on Microwave Theory and Techniques*, Vol. 56, No. 11, (Nov. 2008), pp. 2574-2581.
- BO, P., YOON, Y., PAPAPOLYMEROU, J., TENTZERIS, M. M. & ALLEN, M. G. (2005). A high performance surface-micromachined elevated patch antenna. *Proceedings of IEEE Antennas and Propagation Society International Symposium, (2005)*, Vol. 1B, pp. 397-400, Washington DC, 3-8 July 2005.
- CHEN, N. Z. N. (2008). Wideband microstrip antennas with sandwich substrate. *IET Microwaves, Antennas and Propagation*, Vol. 2, No. 6, (Sep. 2008), pp. 538-546.
- CROQ, F. & POZAR, D. M. (1991). Millimeter-wave design of wide-band aperture-coupled stacked microstrip antennas. *IEEE Transactions on Antennas and Propagation*, Vol. 39, No. 12, Part 1, (Dec. 1991), pp. 1770-1776.
- DU PONT INC., Summary of Properties for Kapton Polyimide. [Online]. Available: http://www2.dupont.com/Kapton/en_US/index.html.
- GAUTHIER, G. P., COURTAY, A. & REBEIZ, G. M. (1997). Microstrip antennas on synthesized low dielectric-constant substrates. *IEEE Transactions on Antennas and Propagation*, Vol. 45, No. 8, (Aug. 1997), pp. 1310-1314.
- HOU, F., ZHU, J., YU, Y.-W. & WU, J. (2008). Millimeter-wave design of aperture-coupled micromachined patch antennas. *Proceedings of the International Conference on Microwave and Millimeter Wave Technology (ICMMT 2008)*, pp. 1401-1404, Nanjing, China, 21-24 Apr. 2008.
- HUANG, C. U., CHEN, I. Y., CHEN, H. J. H., JOU, C. F. & HUANG, S. R. S. (2005). Compact 3D-MEMS-meander monopole antenna. *Electronics Letters*, Vol. 41, No. 21, (Oct. 2005), pp. 1149-1151.
- JAMES, J. R. & HALL, P. S. (1989). *Handbook of microstrip antennas*, IET, ISBN 978-0863411502, London.
- KOUL, S. K. (2007). Design and development of passive and active RF components using MEMS technology. *Proceedings of International Workshop on Physics of Semiconductor Devices (IWPSD 2007)*, pp. 670-675, Bombay, India, 16-20 Dec. 2007.
- KRATZ, H. & STENMARK, L. (2005). Micromachined S-band patch antenna with reduced dielectric constant. *Proceedings of the 13th International Conference on Transducers, Solid-State Sensors, Actuators and Microsystems*, pp. 1088-1091, Seoul, Korea, 5-9 June 2005.

- LEUNG, L. L. W., CHEN, K. J., HUO, X. & CHAN, P. C. H. (2002). On-Chip microwave filters on standard silicon substrate incorporating a low-k BCB dielectric layer. *Proceedings of the 32nd European Microwave Conference*, pp. 1-4, Milan, Italy, Oct. 2002.
- LUCYSZYN, S. (2001). Comment: Terahertz time-domain spectroscopy of films fabricated from SU-8. *Electronics Letters*, Vol. 37, No. 20, (Sep. 2001), pp. 1267-1267.
- MENDES, P. M., POLYAKOV, A., BARTEK, M., BURGHARTZ, J. N. & CORREIA, J. H. (2006). Integrated chip-size antennas for wireless microsystems: Fabrication and design considerations. *Sensors and Actuators A: Physical*, Vol. 55, No. 2, (2006), pp. 217-222.
- MESTDAGH, S., WALTER DE, R. & VANDENBOSCH, G. A. E. (2004) CPW-fed stacked microstrip antennas. *IEEE Transactions on Antennas and Propagation*, Vol. 52, No. 1, (Jan. 2004), pp. 74-83.
- OJEFORS, E., KRATZ, H., GRENIER, K., PLANA, R. & RYDBERG, A. (2006). Micromachined loop antennas on low resistivity silicon substrates. *IEEE Transactions on Antennas and Propagation*, Vol. 55, No. 12, (Dec. 2006), pp. 3593-3601.
- PAN, B., YOON, Y. K., PONCHAK, G. E., ALLEN, M. G., PAPAPOLYMEROU, J. & TENTZERIS, M. M. (2006). Analysis and characterization of a high-performance Ka-band surface micromachined elevated patch antenna. *IEEE Antennas and Wireless Propagation Letters*, Vol. 5, No. 1, (Dec. 2006), pp. 511-514.
- PAPAPOLYMEROU, I., FRANKLIN DRAYTON, R. & KATEHI, L. P. B. (1998). Micromachined patch antennas. *IEEE Transactions on Antennas and Propagation*, Vol. 46, No. 2, (Feb. 1998), pp. 275-283.
- PATEL, J. N., KAMINSKA, B., GRAY, B. L. & GATES, B. D. (2008). PDMS as a sacrificial substrate for SU-8-based biomedical and microfluidic applications. *Journal of Micromechanics and Microengineering*, Vol. 18, No. 9, (Sep. 2008), pp. 095028/1-095028/11.
- PAVULURI, S. K., WANG, C. H. & SANGSTER, A. J. (2008). A high-performance aperture-coupled patch antenna supported by a micromachined polymer ring. *IEEE Antennas and Wireless Propagation Letters*, Vol. 7, (2008), pp. 283-286.
- POZAR, D. M. (1985) Microstrip antenna aperture-coupled to a microstripline. *Electronics letters*, Vol. 21, No. 2, (Jan. 1985), pp. 49-50.
- POZAR, D. M. (1992) Microstrip antennas. *Proceedings of the IEEE*, Vol. 80, No. 1, (Jan. 1992), pp. 79-91.
- RYO-JI, T. & KUROKI, F. (2007). High permittivity tape transmission line embedded in low dielectric support at millimeter-wave frequencies. *Proceedings of the Microwave Conference*, (KJMW 2007), pp. 189-192, Okinawa, Japan, 15-16 Nov. 2007.
- SCHULER, K., VENOT, Y. & WIESBACK, W. (2003). Innovative material modulation for multilayer LTCC antenna design at 76.5 GHz in radar and communication applications. *Proceedings of the 33rd European Microwave Conference*, Vol. 2, pp. 707-710, Munich, Germany, 7-9 Oct. 2003.
- TACONIC, SPECIALIZING IN COATING OF GLASS FABRICS WITH PTFE ([Online]. Available: <http://www.taconic-add.com/pdf/tly.pdf>) Data sheet for TLY RF & Microwave Laminate. *Woven fiber glass fabric coated with PTFE interleaved with thin sheets of pure PTFE.*

- THOMPSON, D. C., TANTOT, O., JALLAGEAS, H., PONCHAK, G. E., TENTZERIS, M. M. & PAPAPOLYMEROU, J. (2004). Characterization of liquid crystal polymer (LCP) material and transmission lines on LCP substrates from 30 to 110 GHz. *IEEE Transactions on Microwave Theory and Techniques*, Vol. 52, No. 4, (April 2004), pp. 1343-1352.
- THORPE, J. R., STEENSON, D. P. & MILES, R. E. (1998). High frequency transmission line using micromachined polymer dielectric. *Electronics Letters*, Vol. 34, No. 12, (June 1998), pp. 1237-1238.
- TONG, K. F., AU, T. M., LUK, K. M. & LEE, K. F. (1995). Wideband two-layer five-patch microstrip antennas. *Digest of the International Symposium on Antennas and Propagation Society*, Vol. 4, pp. 2112-2115, California, 18-23 June 1995.
- TUOMIKOSKI, S. & FRANSSILA, S. (2005). Free-standing SU-8 microfluidic chips by adhesive bonding and release etching. *Sensors and Actuators A: Physical*, Vol. 120, No. 2, (Feb. 2005), pp. 408-415.
- WANG, C. H. & PAVULURI, S. K. (2008). Fabrication and assembly of high gain MEMS antennas for wireless communications. *Proceedings of the 58th Electronic Components and Technology Conference (ECTC 2008)*, pp. 1941-1945, Florida, 26-29 May 2008.
- WANG, J., CAI, Y., ATIVANICHAYAPHONG, T., CHIAO, M. & CHIAO, J. C. (2005). Fabrication techniques and RF performances of transmission lines on polymer substrates. *SPIE Proceedings of Conference on Microelectronics: Design, Technology, and Packaging II*, pp. 60351M.1-60351M.9), Brisbane, Australia, Dec. 2005.
- WI, S. H., KIM, J. S., KANG, N. K., KIM, J. C., YANG, H. G., KIM, Y. S. & YOON, J. G. (2007). Package-level integrated LTCC antenna for RF package application. *IEEE Transactions on Advanced Packaging*, Vol. 30, No. 1, (Feb. 2007), pp. 132-141.
- WOLFF, I. (2007). Design and technology of microwave and millimeter wave LTCC circuits and systems. *Proceedings of the International Symposium on Signals, Systems and Electronics*, pp. 505-512, Montreal, Canada, 30 July - 2 Aug. 2007.
- ZÜRCHER, J.-F. (1988). The SSFIP: A global concept for high performance broadband planar antennas. *Electronics letters*, Vol. 24, No. 23, (Nov. 1998), pp. 1433-1435.



Mobile and Wireless Communications Network Layer and Circuit Level Design

Edited by Salma Ait Fares and Fumiyuki Adachi

ISBN 978-953-307-042-1

Hard cover, 404 pages

Publisher InTech

Published online 01, January, 2010

Published in print edition January, 2010

Mobile and wireless communications applications have a clear impact on improving the humanity wellbeing. From cell phones to wireless internet to home and office devices, most of the applications are converted from wired into wireless communication. Smart and advanced wireless communication environments represent the future technology and evolutionary development step in homes, hospitals, industrial, vehicular and transportation systems. A very appealing research area in these environments has been the wireless ad hoc, sensor and mesh networks. These networks rely on ultra low powered processing nodes that sense surrounding environment temperature, pressure, humidity, motion or chemical hazards, etc. Moreover, the radio frequency (RF) transceiver nodes of such networks require the design of transmitter and receiver equipped with high performance building blocks including antennas, power and low noise amplifiers, mixers and voltage controlled oscillators. Nowadays, the researchers are facing several challenges to design such building blocks while complying with ultra low power consumption, small area and high performance constraints. CMOS technology represents an excellent candidate to facilitate the integration of the whole transceiver on a single chip. However, several challenges have to be tackled while designing and using nanoscale CMOS technologies and require innovative idea from researchers and circuits designers. While major researchers and applications have been focusing on RF wireless communication, optical wireless communication based system has started to draw some attention from researchers for a terrestrial system as well as for aerial and satellite terminals. This renewed interested in optical wireless communications is driven by several advantages such as no licensing requirements policy, no RF radiation hazards, and no need to dig up roads besides its large bandwidth and low power consumption. This second part of the book, Mobile and Wireless Communications: Key Technologies and Future Applications, covers the recent development in ad hoc and sensor networks, the implementation of state of the art of wireless transceivers building blocks and recent development on optical wireless communication systems. We hope that this book will be useful for students, researchers and practitioners in their research studies.

How to reference

In order to correctly reference this scholarly work, feel free to copy and paste the following:

Sumanth K. Pavuluri, Changhai Wang and Alan J. Sangster (2010). Micromachined High Gain Wideband Antennas for Wireless Communications, Mobile and Wireless Communications Network Layer and Circuit Level Design, Salma Ait Fares and Fumiyuki Adachi (Ed.), ISBN: 978-953-307-042-1, InTech, Available from: <http://www.intechopen.com/books/mobile-and-wireless-communications-network-layer-and-circuit-level-design/micromachined-high-gain-wideband-antennas-for-wireless-communications>

INTECH

open science | open minds

InTech Europe

University Campus STeP Ri
Slavka Krautzeka 83/A
51000 Rijeka, Croatia
Phone: +385 (51) 770 447
Fax: +385 (51) 686 166
www.intechopen.com

InTech China

Unit 405, Office Block, Hotel Equatorial Shanghai
No.65, Yan An Road (West), Shanghai, 200040, China
中国上海市延安西路65号上海国际贵都大饭店办公楼405单元
Phone: +86-21-62489820
Fax: +86-21-62489821